DEUTSCHES ELEKTRONEN-SYNCHROTRON DESY

DESY 88-117
August 1988

CALCULATIONS OF DOSES DUE TO ELECTRON-PHOTON STRAY RADIATION FROM A HIGH-ENERGY ELECTRON BEAM BEHIND LATERAL SHIELDING

by

H. Dinter, J. Pang, K. Tesch

Deutsches Elektronen-Synchrotron DESY, Hamburg

ISSN 0418-9833

NOTKESTRASSE 85 · 2 HAMBURG 52

To be sure that your preprints are promptly included in the
HIGH ENERGY PHYSICS INDEX ,
send them to the following address (if possible by air mail) :

DESY
Bibliothek
Notkestrasse 85
2 Hamburg 52
Germany

DESY 88-117
August 1988

ISSN 0418-9833

Calculations of Doses Due to Electron–Photon Stray Radiation from a High–Energy Electron Beam Behind Lateral Shielding

H. Dinter, J. Pang*, K. Tesch
Deutsches Elektronen-Synchrotron DESY,
D-2000 Hamburg 52, F. R. Germany

Abstract

Doses due to stray radiation produced by high-energy electrons are calculated for the shielding materials lead, iron, heavy and ordinary concrete, and sand. Source terms and absorption coefficients were determined using the Monte Carlo program EGS4 for 12 different target configurations and for the target materials iron and aluminium. The dependencies on the primary energy, target configurations, and angle of observation were studied. The results are compared with experimental values at 5 GeV; the agreement is good. The results are parametrised to facilitate dose calculations.

1 Introduction

1.1 General Remarks

The shielding of a high-energy particle accelerator is a problem which concerns both radiological and economical aspects. Detailed knowledge of the mechanisms of interaction of particles with matter, of the composition of the radiation fields, and the propagation of stray radiation through various types of absorbers is necessary in order to design and to optimise the arrangement of shielding materials.

In the case of electron accelerators (to which we will confine ourselves) several components contribute to the radiation field which has to be shielded. The component producing the highest contribution to the dose behind a shield of moderate thickness is a mixture of photons, electrons and positrons originating from electromagnetic interactions (production of bremsstrahlung, Compton-effect, pair production, etc.). Other components are neutrons or muons which are created by high-energy photons. These particles are more penetrating than the electromagnetic ones; their contribution to the dose begins to dominate only behind a relatively thick layer of shielding material. They will not be considered in this report.

*On leave of absence from the Institute of Plasma Physics, Academia Sinica, Hefei, China

Three problems are encountered when calculating dose levels behind shielding:

1. A precise knowledge of the physics of all interaction processes is necessary — in our case of the electromagnetic processes,

2. the geometry of the problem has to be defined and simplified in such a way that calculations can be performed, and

3. the rate of interacting primary particles must be known.

Point three cannot be treated in a general way. In most cases these values are more or less unknown. Hence assumptions have to be made for different scenarios of beam losses, which is a problem that has to be solved individually for each accelerator. In most cases uncertainties resulting from this point determine the accuracy of the dose calculations.

In the past some experiments were performed to obtain basic data for shielding calculations[1,2]. "Basic data" generally means:

- the dose caused by one primary particle in a certain distance from a source ("source term"), and

- absorption coefficients of common materials with respect to this dose.

The experimental data do not cover all requirements for practical applications and therefore inter- or extrapolations have to be made to obtain appropriate values.

Therefore, in this report

1. basic shielding data are calculated by use of an established Monte Carlo program, and compared with the experimental data of Reference 1,

2. the most relevant dependencies of source terms and attenuation coefficients are studied, and

3. a simple formula for calculating the doses is presented.

1.2 Method of Calculation

The Monte Carlo program used was EGS4. It has proven ability to calculate the processes of the electromagnetic interactions in many cases[3]. EGS4 itself serves as a subprogram; it manages the transport of the particles. The user has to add a main program for all initialisations, where the actual geometry and the distribution of various materials are defined, and the final EGS-data are evaluated.

For the present problem EGS4 was used twice:

- In the *first step* primary electrons hit a target and produce secondary particles (electrons, photons, and positrons) which are binned with respect to their angle of emittance. In this way spectra of this stray radiation are obtained as a function of the angle of observation, and an angular distribution of the dose can be calculated for a given distance.

- In the *second step* a beam of particles is incident perpendicularly to a rectangular block of material. The composition of the beam and the energy of the particles correspond to those of the stray radiation produced in step 1 belonging to a particular angle of observation. The penetration of the particles into the absorber is followed and the dose calculated as a function of the absorber thickness.

All calculated dose values are determined by the energy deposited by ionising particles (electrons and positrons) in tissue.

2 Production of Stray Radiation

2.1 Arrangement and Procedure

The geometrical arrangement is shown in Figure 1. A one-dimensional beam of monoenergetic electrons (energy E_{pr}) hits a target. The target is a slab of material with thickness d whose parallel surface planes are oriented with respect to the beam direction by an angle φ. The stray radiation is "observed" at an angle θ. Both angles, φ and θ, are defined in a plane perpendicular to the target surface. They are regarded to be positive on the right hand of the beam axis and negative on the left.

EGS controls the three-dimensional development of the cascade within the target and produces secondary particles. When leaving the target, the angle θ is calculated for each particle from its flight direction, and added to the spectrum in the appropriate bin (the 360 degrees around the centre of the target are divided into 22 θ-bins of different sizes).

The most suitable energy cuts applied to EGS were investigated. They are chosen as high as possible to save CPU-time, and as low as necessary in order not to influence the calculated dose values. The best values turned out to be 500 keV kinetic energy for charged particles, and 10 keV for photons.

For practical purposes the most interesting target material is iron, hence most of the calculations were performed for this material. In addition some calculations were repeated for aluminium (see Chapter 4). Thicknesses and orientations of iron targets were varied from 2 mm (e.g. the thickness of a beam pipe) to 10 cm (simulation of a magnet), and from grazing incidence (0.1^0) to the case of beam absorbers (90^0).

For the most common target configurations the energy of the electron beam was varied between 150 MeV and 50 GeV.

The investigated combinations of E_{pr}, d and φ are summarised in Table 1.

All calculations were performed on an IBM 3084Q computer.

2.2 Angular Dose Distribution

In Reference 1 some angular dose distributions around unshielded targets were measured at 5 GeV. These curves now serve as a check of EGS4 and the associated code, giving confidence to continue investigation.

In Figure 2 we selected the example of $d = 0.2$ cm and $\varphi = -10^0$ for a primary energy of 5 GeV. The dose values are plotted against the angle of observation for the total 360 degrees. The measured doses of Reference 1 are shown as a smooth line to guide the eye. The calculated doses are shown together with the widths of the angle bins and error bars. These bars

represent the standard deviations of the doses obtained from 10 Monte Carlo runs each of 10 minutes CPU-time.

The dose values were calculated for a layer of tissue material with a thickness of 0.5 cm. The doses are due either to incoming electrons or positrons, or to electrons released by photons within the tissue. However, the probability of interaction of a photon is very small in such a thin layer and cannot be calculated within a reasonable CPU-time. The contribution of photons to the dose can be taken into account by calculating their kerma, knowing that their dose is overestimated in this way. However, for angles less than 90^0 the dose is highly dominated by charged particles, and photons need not be taken into account (see Figure 5). Even for backward directions their contribution only amounts to less than 5%, and the overestimation may be neglected.

In general, the agreement between experimental and calculated doses is better than a factor of 2 over $3\frac{1}{2}$ orders of magnitude. This is also valid for other target configurations. The dip in the distribution around $\theta = -20^0$ originates from the coincidence of target orientation and direction of observation. The agreement could be improved in that region simply by diminishing the widths of the angle bins.

In Table 2 the numerical values of the calculated doses are listed for 4 values of θ and for all investigated target configurations.

2.3 Spectra of Secondary Radiation

In the way described above, the fluences of secondary particles, normalized to one incoming electron, are calculated for all 22 bins of the angle θ. In Figures 3 and 4 spectra are shown for 4 angles for the target d = 0.2 cm and $\varphi = -2^0$. In both cases the fluences are plotted in lethargy units. In this way the area under the histograms are proportional to the fluences.

The peaked forward intensity of both types of secondary particles can be clearly seen. In the case of photons the annihilation peak at 511 keV is found to be independent of θ and as expected is more pronounced in backward directions.

The shape of the spectra depends on the target configuration, especially on the variable $w = d/\sin\varphi$ which is a measure for the development of the cascade. On the contrary, the shape of the spectra does not change when varying the primary energy; only the total fluence varies.

3 Absorption of Stray Radiation

3.1 Arrangement and Procedure

The simulation was arranged as follows: The material in which the absorption of the stray radiation is to be studied, was positioned in a series of 10 parallel slabs (20×20 cm^2), separated by thin layers of tissue material ("detectors") in which the doses are to be calculated (5×5 cm^2; 0.2 cm thick).

The particles were arranged to impinge perpendicularly to the absorber stack. The "beam" was adjusted to have the same cross-section as the detectors (5×5 cm^2) in order to save computer time.

Corrections have to be applied for this limited beam size. Other corrections must be made for the finite thicknesses of the detectors. Thick detectors cause an additional decrease of the

doses because the distance from the incidence of the particles to a detector is higher than the thickness of the absorber between these two points. Both corrections depend on the absorber material; they are of the order of 10%.

The most common shielding materials are lead, iron, concrete (heavy and ordinary), and sand (or soil). The following calculations were performed for these materials. Their data are summarised in Table 3. For each material the dose was calculated at 11 locations within the absorber stack. The primary energy, the target configuration, and the angle of observation were varied.

3.2 Absorption coefficients

If the calculated doses are plotted in a semilogarithmic scale against the absorber thickness, a steep decrease within the first centimeters of the absorber is observed, with an exponential attenuation following this decay.

In Figure 5 this is demonstrated for the example of an iron absorber bombarded with stray radiation at 30^0. The radiation stems from an 0.2 cm thick iron target positioned at -2^0 to a 5 GeV-electron beam. In addition experimental dose values from Reference 1 are displayed for comparison in Figure 5. The agreement is quite good. The error bars of the calculated values represent errors of mean values of 5 MC-runs, each of 10 minutes.

For a better understanding of the absorption mechanisms, kerma values produced by photons when entering a "detector" are also displayed in figures. Unlike the doses, the kerma values show a small build-up in the first centimeters of the absorber. However, the exponential decay is reproduced in the same way.

Thus it may be concluded that the steep decay is due to the absorption of the incoming charged particles. In fact, as may be seen in Figure 4 for our example, the number of charged particles at 30^0 is very small above 75 MeV. This energy corresponds to an electron range in iron of 3 cm, all incoming electrons being absorbed after traversing this absorber thickness.

The doses at thicknesses higher than the range of incoming charged particles are due to electrons produced by photons ("secondary electrons"). These electrons are in equilibrium with the photons, and kerma and dose should be equivalent. This indeed agrees with the calculations as can be seen in Figure 5.

Although producing a dose of the same amount as the kerma, the number of electrons is small compared with that of the photons, and therefore the statistical fluctuations of the doses are much higher than those of the kerma values. However, since the kerma values show the same exponential attenuation as the doses, they were used for the determination of the absorption coefficients, resulting in a much higher accuracy than if the dose values had been used.

The following results concerning the absorption coefficient λ were obtained:

Dependence on primary energy: The dependence of λ on E_{pr} was investigated for a single target configuration (d = 0.2 cm; $\varphi = -0.5^0$) and for iron absorbers. It was found that λ is independent of the primary energy in the range 0.5 to 15 GeV. This result is in agreement with the statement in Section 2.3 concerning the independence of the particle spectra of the primary energy. The numerical values of λ are listed in Table 4 for 3 angles of observation.

Dependence on the target configuration: For 5 configurations (w ranging between 5.7 and 23 cm) absorption coefficients were calculated for all considered absorber materials. Results for $\theta = 25^0$ are shown in Table 5. No significant dependence was observed. Therefore the λ-values were averaged over all target configurations. The uncertainties represent errors of mean values.

Dependence on the angle of observation: When looking at the spectra of Figures 3 and 4, a dependence of λ on the angle θ is expected. In Table 6 the results of the calculations are displayed for 3 angles. A small increase of the absorption coefficient with higher angles is visible, especially in the case of light absorption materials (for lead no such increase could be found). However regarding the uncertainties, the differences are low and for most applications the use of a mean absorption coefficient can be recommended. Such mean values are found in column 5 of Table 6 together with the coefficients of Reference 1 (column 6). The agreement is good, in most cases even within the quoted limits. Only for heavy concrete is the measured value 15 % lower than the calculated one.

3.3 Source Terms

According to absorption curves produced in Section 3.2 (e. g. Figure 5), the dose behind a certain thickness of absorber material can be calculated using an exponentially decreasing factor and a source term (and of course the distance between source and point of interest).

Usually the expression "source term" means the dose value H_0 in front of the absorber (at thickness zero). In this case, the strong absorption of the dose within the first centimeters of the material has to be accounted for (which has been done in Reference 1 by introducing a reduction factor A_T). In this report another approach is followed:

We proved in detailed calculations that the dose H_A behind a certain absorber thickness x_A (the point where the exponential decay begins) is almost independent of the absorber material. The value of x_A depends on the material but the product $x_A \cdot \rho$ is independent and was determined to be 75 g/cm^2 (ρ being the density of the absorber).

An accelerator for high-energy particles never can be operated without shielding; the thickness of shielding material must significantly exceed 75 g/cm^2. Therefore the knowledge of the dose in front of the shielding and of reduction factors (which depend on the target and θ) is unnecessary. It is more convenient to use only a single source term H_A (being the same value for all absorbers), and to commence the calculation of the exponential decay at $x_A \cdot \rho$.

The independence of H_A of absorber materials is demonstrated in Table 7 for the angle 25^0. The agreement is fairly good except for lead where the calculated doses will be overestimated if the average value is used.

The source term H_A was studied carefully and the following properties can be summarised:

Dependence on primary energy: For a series of target configurations, the energy dependence of H_A was investigated. For one example (d = 0.2 cm; $\varphi = -0.5^0$), the calculated H_A-values are plotted as a function of the primary energy in Figure 6. The double logarithmic plots show that a fit of the type $H \sim E^\alpha$ is possible in the energy range 150 MeV to 50 GeV.

The evaluation of all fits results in the α-values of Table 8. The exponent α depends on $w = d/\sin\varphi$ in a simpler way than on d or φ , but it does not depend significantly on the angle

θ. Exponents averaged over the angle θ are recommended for use and are given in column 7 of Table 8.

A plot of α against w reveals a simple logarithmic increase up to w = 20 cm approaching a saturation value around 1.2 (Figure 7).

Dependence on the target configuration: We calculated H_A for 12 target configurations at an energy of 5 GeV. The results are given in Table 9. The average standard deviation is 20 %. Plots of the H_A-values prove that between $\theta = 7.5^0$ and 90^0 (other angles were not considered) and for w $\leq$ 10 cm they depend only on w and in a way that permits a fit of the type $H_A \sim w^\beta$ (Figure 8). A best value of $\beta = 2.5$ was found. For w > 10 cm no such simple dependence could be found, and the H_A-values have to be taken from Table 9.

Dependence on the angle of observation: From Figure 8 the dependence on the angle of observation can also be deduced. The w-fits are shown as straight lines in the double logarithmic plots. These lines are more or less parallel for all three angles. Thus in the same range as before an analog fit $H \sim (\theta/\theta_0)^\gamma$ can be made. The best value obtained for the exponent was $\gamma = -3.8$ with $\theta_0 = 7.5^0$.

4 Aluminium as Target Material

For some applications the use of aluminium is prefered to iron. Aluminium is a common material for vacuum chambers, and a practical problem is the grazing incidence of a beam on the surface of such a chamber. Therefore additional calculations were performed for a target thickness of 0.2 cm and angles of incidence between 0.1^0 and 10^0.

4.1 Spectra and Absorption Coefficients

Following the same procedure as in the case of the iron targets, spectra of secondary particles were calculated. In general the shape of the spectra are very similar to those resulting from iron targets, but the fluences are much lower.

Thus the absorption coefficients are the same as calculated in Section 3.2 (Table 6), within the usual limits of uncertainty.

4.2 Source Terms

Due to the lower intensity of secondary particles from aluminium targets, the source terms are smaller than in the case of the corresponding iron targets. In Figure 9, the values of H_A are plotted against w similar to Figure 8. Again fits of the type $H \sim w^\beta$ may be applied, but in contrast to iron at least up to w = 115 cm. The numerical values of H_A are found in Table 10.

The dependency on the primary energy was not studied. It is assumed to be the same as in the case of the iron targets.

5 Results

Taking into account the results of the Sections 3.2 and 3.3, the dose behind shielding material can be calculated in the following way:

$$H = H_A(E_{pr}, d, \varphi, \theta) \cdot (\frac{r_0}{r})^2 \cdot e^{-\lambda(\theta)\cdot(x\rho - x_A\rho)}$$

where $x_A\rho = 75$ g/cm^2, $r_0 = 1$ m. The other symbols are explained in Figure 1.

The results can be summarised in the following form:

Energy dependence: The energy dependence may be separated from the source term:

$$H_A(E_{pr}, d, \varphi, \theta) = (\frac{E_{pr}}{E_0})^\alpha \cdot H'_A(d, \varphi, \theta)$$

where $E_0 = 5$ GeV. The exponent α may be taken from Table 8 as a function of the angle θ or as an averaged value. It depends on w ($w = d/\sin\varphi$); the dependence is displayed in Figure 7.

Dependence on target configuration and angle of observation: Values $H'_A(d, \varphi, \theta)$ can be found in Table 9 for iron targets and in Table 10 for aluminium targets. They may be applied to shielding thicknesses of $x \geq 75$ g/cm^2. For iron targets with $w \leq 10$ cm or aluminium targets with $w \leq 115$ cm, and θ between 5° and 100°, H'_A may be expressed as a function of w and θ only and can be parametrised in the following way:

$$H'_A(w, \theta) = H^0_A \cdot (\frac{w}{w_0})^\beta \cdot (\frac{\theta}{\theta_0})^\gamma$$

where

$H^0_A = (3.2 \pm 0.2) \cdot 10^{-15}$ Gy/primary electron – for iron targets,
$H^0_A = (9.6 \pm 1.0) \cdot 10^{-17}$ Gy/primary electron – for aluminium targets,

$w_0 = 1$ cm,
$\beta(\mathrm{Fe}) = 2.5$,
$\beta(\mathrm{Al}) = 2.2$,

$\theta_0 = 7.5°$,
$\gamma(\mathrm{Fe}) = -3.8$ and
$\gamma(\mathrm{Al}) = -4.4$.

Absorption coefficients: The absorption coefficients are found to be independent of the primary energy and the target configuration. The numeric values are given in Table 6.

Final remarks: We found good agreement between calculated data and the measurements from Reference 1. The doses H_0 in front of the absorber agree within a factor of 2 with the experimental values (see Figure 2). The absorption coefficients agree with the experimental λ values within the limits of uncertainty with the exception of heavy concrete — in this case we believe that the calculated value is the more realistic one (see Table 6). Calculated doses behind shielding materials tend to be lower than those measured in our earlier experiment. Behind thicknesses of practical interest they are lower by an average factor of 2 to 3.

6 References

1. Dinter, H., and Tesch, K. *Dose and Shielding Parameters of Electron - Photon Stray Radiation for a High Energy Electron Beam.* Nucl. Instr. and Methods 143, 349-355 (1977)

2. Jenkins, T.M. *Neutron and Photon Measurements Through Concrete from a 15 GeV Electron Beam on a Target — Comparisons with Models and Calculations.* Nucl. Instr. and Methods 159, 265-288 (1979)

3. Nelson, W.R., Hirayama, H., and Rodgers, D. W. O. *The EGS4 Code System.* SLAC – Report – 265 (1985), Stanford Linear Accelerator Centre.

d	φ	w	E_{pr} in GeV					
cm	deg	cm	0.15	0.50	1.50	5.00	15.0	50.0
0.2	-0.1	115.		×	×	×	×	
0.2	-0.5	22.9	×	×	×	×	×	×
0.2	-2.0	5.73	×	×	×	⊗	×	×
0.2	-10.	1.15				⊗		
0.2	90.	0.20				⊗		
1.0	-0.5	115.				×		
1.0	-2.0	28.6		×	×	⊗	×	
1.0	-10.	5.76		×	×	⊗	×	
1.0	90.	1.00		×	×	⊗	×	
10.	-2.0	287.				×		
10.	-10.	57.6				⊗		
20.	90.	20.0				×		

Table 1: Target configurations and primary energies; × = calculations of spectra performed; ⊗ = calculations and experimental data available; w = d/sinφ (cf. Figure 1).

d	φ	w	H_0 in Gy/primary electron			
cm	deg	cm	$\theta = (7.5 \pm 2.5)^0$	$\theta = (25. \pm 5.0)^0$	$\theta = (90. \pm 10.)^0$	$\theta = (165. \pm 15.)^0$
0.2	-0.1	115.	$1.7 \cdot 10^{-12}$	$6.3 \cdot 10^{-13}$	$1.2 \cdot 10^{-13}$	$1.9 \cdot 10^{-14}$
0.2	-0.5	22.9	$3.2 \cdot 10^{-12}$	$1.2 \cdot 10^{-12}$	$1.9 \cdot 10^{-13}$	$2.6 \cdot 10^{-14}$
0.2	-2.0	5.73	$2.6 \cdot 10^{-12}$	$6.9 \cdot 10^{-13}$	$9.8 \cdot 10^{-14}$	$1.1 \cdot 10^{-14}$
0.2	-10.	1.15	$9.1 \cdot 10^{-14}$	$1.7 \cdot 10^{-14}$	$2.4 \cdot 10^{-15}$	$3.1 \cdot 10^{-16}$
0.2	90.	0.20	$4.3 \cdot 10^{-15}$	$1.1 \cdot 10^{-15}$		$1.1 \cdot 10^{-17}$
1.0	-0.5	115.	$4.4 \cdot 10^{-13}$	$2.5 \cdot 10^{-13}$	$7.5 \cdot 10^{-14}$	$1.4 \cdot 10^{-14}$
1.0	-2.0	28.6	$1.2 \cdot 10^{-12}$	$5.3 \cdot 10^{-13}$	$1.3 \cdot 10^{-13}$	$1.7 \cdot 10^{-14}$
1.0	-10.	5.76	$1.7 \cdot 10^{-12}$	$4.4 \cdot 10^{-13}$	$6.1 \cdot 10^{-14}$	$5.0 \cdot 10^{-15}$
1.0	90.	1.00	$5.6 \cdot 10^{-14}$	$7.2 \cdot 10^{-15}$		$2.4 \cdot 10^{-17}$
10.	-2.0	287.	$2.4 \cdot 10^{-14}$	$4.7 \cdot 10^{-15}$	$2.5 \cdot 10^{-15}$	$6.0 \cdot 10^{-15}$
10.	-10.	57.6	$6.2 \cdot 10^{-15}$	$1.2 \cdot 10^{-14}$	$6.1 \cdot 10^{-15}$	$1.5 \cdot 10^{-15}$
20.	90.	20.0	$4.0 \cdot 10^{-13}$	$7.8 \cdot 10^{-14}$		$6.6 \cdot 10^{-16}$

Table 2: Angular distribution of the dose H_0 ; primary energy = 5 Gev; iron target; distance = 1 m; w = d/sinφ (cf. Figure1).

Material	Density	Composition
	g/cm^3	% Weight
Lead	11.35	Pb 100.
Iron	7.86	Fe 100.
Heavy Concrete	3.70	Fe 50.5; O 34.4; Si 6.8; Ca 4.8; Mg 1.9; Al 1.0; H 0.4; Mn 0.1
Ordinary Concrete	2.42	O 53.0; Si 34.0; Ca 4.0; Al 3.0; Na 2.0; Fe 2.0; H 1.0; C 1.0
Sand (Soil)	1.60	Si 78.0; O 22.0

Table 3: Material data of the absorbers.

E_{pr}	λ in cm^2/g		
GeV	$\theta = 7.5^0$	$\theta = 25.^0$	$\theta = 90.^0$
0.5	0.027	0.028	0.031
1.5	0.027	0.028	0.032
5.0	0.025	0.029	0.031
15.	0.025	0.027	0.032

Table 4: Attenuation coefficients; dependence on primary energy; iron target: d = 0.2 cm; $\varphi = -0.5°$; absorber material is iron.

d	φ	w	λ in cm^2/g				
cm	deg	cm	Lead	Iron	Heavy Concrete	Ordinary Concrete	Sand
0.2	-0.5	22.9	0.046 ±0.003	0.029 ±0.003	0.027 ±0.002	0.021 ±0.001	0.021 ±0.002
0.2	-2.0	5.73	0.046 ±0.004	0.028 ±0.003			
1.0	-5.0	11.5	0.042 ±0.004	0.027 ±0.003	0.026 ±0.002		0.022 ±0.002
1.0	-10.	5.76	0.045 ±0.003	0.028 ±0.003	0.026 ±0.002	0.022 ±0.001	0.019 ±0.002
20.	90.	20.0	0.043 ±0.003	0.027 ±0.003	0.024 ±0.002	0.021 ±0.001	0.019 ±0.002

Table 5: Attenuation coefficients; dependence on target configuration; primary energy = 5 GeV; $\theta = 25° \pm 5°$.

Material	λ in cm^2/g			$\overline{\lambda}$	$\lambda(1)$
	$\theta = 7.5°$	$\theta = 25.°$	$\theta = 90.°$		
Lead	0.044 ±0.003	0.044 ±0.003	0.044 ±0.003	0.044 ±0.001	0.042
Iron	0.024 ±0.001	0.028 ±0.001	0.031 ±0.002	0.028 ±0.001	0.029
Heavy Concrete	0.024 ±0.002	0.026 ±0.002	0.027 ±0.002	0.026 ±0.001	0.022
Ordinary Concrete	0.020 ±0.001	0.021 ±0.001	0.025 ±0.002	0.022 ±0.001	0.023
Sand	0.019 ±0.002	0.021 ±0.002	0.025 ±0.002	0.022 ±0.001	0.019

Table 6: Recommended attenuation coefficients; $\lambda(1)$ are the absorption coefficients from Reference 1.

Material	Density	x_A	H_A	KERMA
	g/cm^3	cm	Gy/primary electron	Gy/primary electron
Lead	11.35	6.6	$4.1 \cdot 10^{-15}$	$5.3 \cdot 10^{-15}$
Iron	7.86	9.5	$8.9 \cdot 10^{-15}$	$9.2 \cdot 10^{-15}$
Heavy Concrete	3.70	20.	$7.0 \cdot 10^{-15}$	$7.9 \cdot 10^{-15}$
Ordinary Concrete	2.42	31.	$1.0 \cdot 10^{-14}$	$8.8 \cdot 10^{-15}$
Sand	1.60	47.	$6.5 \cdot 10^{-15}$	$8.3 \cdot 10^{-15}$
		average =	$(7.4 \pm 1.1) \cdot 10^{-15}$	$(7.9 \pm 0.7) \cdot 10^{-15}$

Table 7: Dose values H_A and kerma values behind material thickness x_A ($x_A \cdot \rho = 75$ g/cm^2); primary energy = 5 GeV; iron target: d = 0.2 cm; $\varphi = -0.5°$; $\theta = 25° \pm 5°$.

w	d	φ	α			$\overline{\alpha}$	
cm	cm	deg	$\theta = 7.5^0$	$\theta = 25.^0$	$\theta = 90.^0$		
1.0	1.0	90.	0.050 $\pm$0.010	0.045 $\pm$0.045		0.048 $\pm$0.023	
5.73	0.2	-2.0	0.61 $\pm$0.10	0.52 $\pm$0.05	0.51 $\pm$0.03	0.55 $\pm$0.04	*
5.76	1.0	-10.	0.64 $\pm$0.05	0.41 $\pm$0.01	0.51 $\pm$0.04	0.52 $\pm$0.02	
22.9	0.2	-0.5	1.01 $\pm$0.06	1.00 $\pm$0.01		1.00 $\pm$0.03	
28.7	1.0	-2.0	1.05 $\pm$0.04	0.97 $\pm$0.03	0.95 $\pm$0.07	0.99 $\pm$0.03	*
114.	0.2	-0.1	1.10 $\pm$0.05	1.15 $\pm$0.05	1.37 $\pm$0.05	1.21 $\pm$0.03	

Table 8: Energy exponents α in the range 0.5 to 15 GeV; for * from 0.15 to 50 GeV.

w	d	φ	H_A in Gy/primary electron			
cm	cm	deg	$\theta = 7.5^0$	$\theta = 25.^0$	$\theta = 90.^0$	
0.20	0.2	90.	$5.6 \cdot 10^{-17}$	$6.9 \cdot 10^{-19}$	$8.2 \cdot 10^{-21}$	*
1.00	1.0	90.	$2.8 \cdot 10^{-15}$	$3.6 \cdot 10^{-17}$	$7.0 \cdot 10^{-20}$	*
1.15	0.2	-10.	$4.6 \cdot 10^{-15}$	$4.9 \cdot 10^{-17}$	$1.8 \cdot 10^{-19}$	
5.73	0.2	-2.0	$2.3 \cdot 10^{-13}$	$3.5 \cdot 10^{-15}$	$1.3 \cdot 10^{-17}$	
5.76	1.0	-10.	$1.6 \cdot 10^{-13}$	$3.7 \cdot 10^{-15}$	$3.3 \cdot 10^{-17}$	
20.0	20.	90.	$6.6 \cdot 10^{-14}$	$2.7 \cdot 10^{-15}$	$1.5 \cdot 10^{-17}$	*
22.9	0.2	-0.5	$3.0 \cdot 10^{-13}$	$8.7 \cdot 10^{-15}$	$1.1 \cdot 10^{-16}$	
28.6	1.0	-2.0	$1.5 \cdot 10^{-13}$	$3.5 \cdot 10^{-14}$	$4.4 \cdot 10^{-16}$	
57.6	10.	-10.	$7.0 \cdot 10^{-16}$	$1.3 \cdot 10^{-15}$	$9.2 \cdot 10^{-17}$	
115.	0.2	-0.1	$1.6 \cdot 10^{-13}$	$5.0 \cdot 10^{-15}$	$5.1 \cdot 10^{-17}$	
115.	1.0	-0.5	$6.2 \cdot 10^{-14}$	$2.0 \cdot 10^{-14}$	$2.7 \cdot 10^{-16}$	
287.	10.	-2.0	$8.1 \cdot 10^{-19}$	$7.8 \cdot 10^{-17}$	$1.2 \cdot 10^{-16}$	

Table 9: Source terms H_A for iron targets; primary energy = 5 GeV; for * : $\theta = 135^\circ \pm 15^\circ$; the average standard deviation is 20 %.

w	d	φ	H_A in Gy/primary electron		
cm	cm	deg	$\theta = 7.5^0$	$\theta = 25.^0$	$\theta = 90.^0$
1.15	0.2	-10.	$1.3 \cdot 10^{-16}$	$1.1 \cdot 10^{-18}$	$2.2 \cdot 10^{-21}$
5.73	0.2	-2.0	$5.1 \cdot 10^{-15}$	$3.6 \cdot 10^{-17}$	$6.0 \cdot 10^{-20}$
22.9	0.2	-0.5	$7.3 \cdot 10^{-14}$	$5.5 \cdot 10^{-16}$	$1.3 \cdot 10^{-19}$
115.	0.2	-0.1	$2.3 \cdot 10^{-12}$	$1.3 \cdot 10^{-14}$	$3.7 \cdot 10^{-17}$

Table 10: Source terms H_A for aluminium targets; primary energy = 5 GeV; the average standard deviation is 25 %.

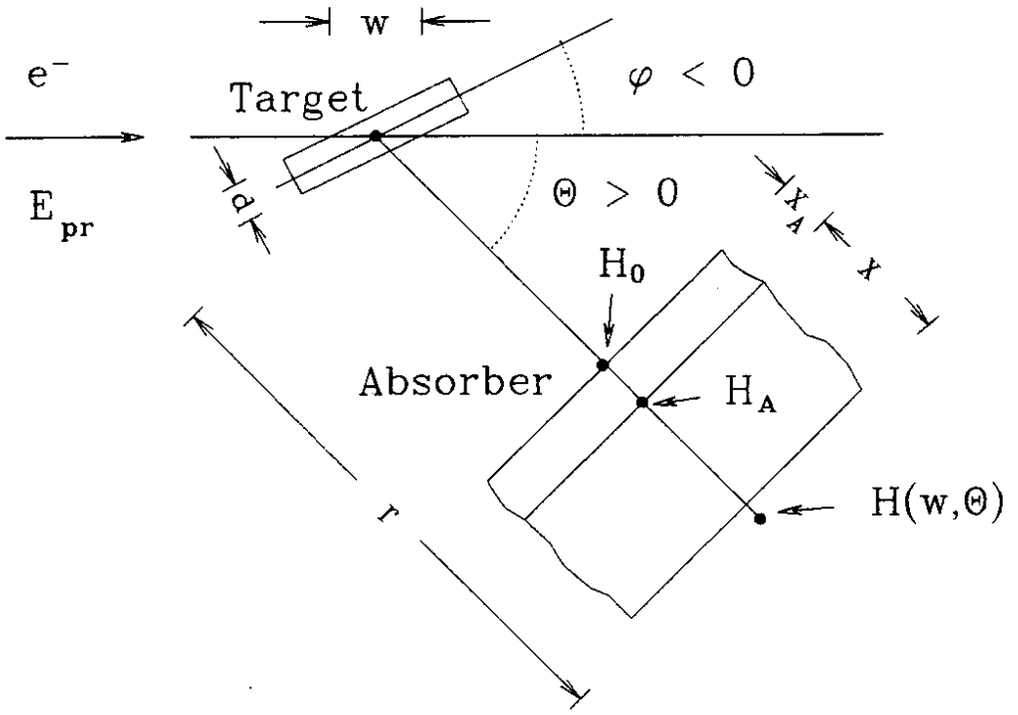

Figure 1: Target and absorber arrangement.

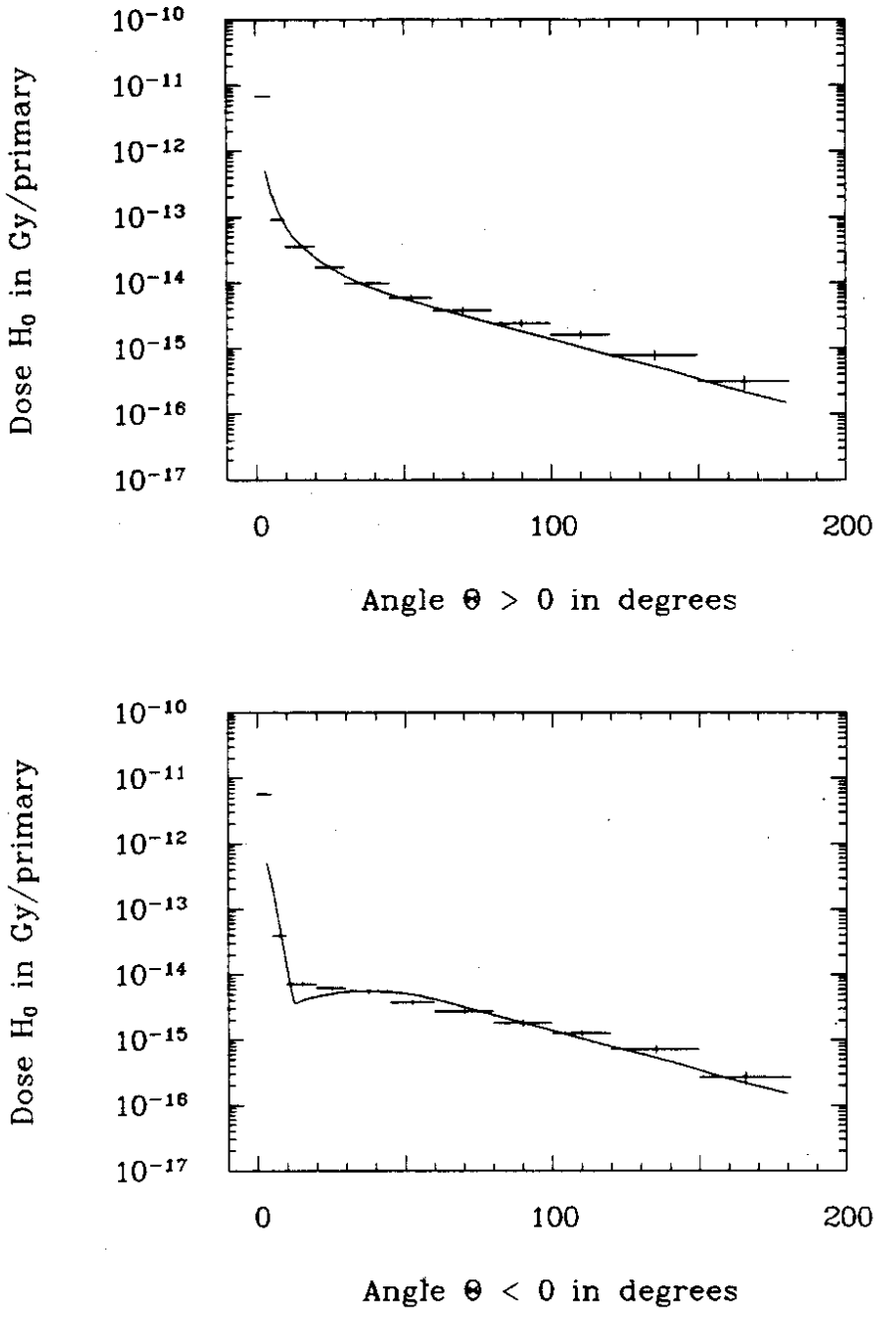

Figure 2: Angular distribution of dose H_0 (unshielded target cf. Figure 1); primary energy = 5 GeV; iron target: d = 0.2 cm; $\varphi = -10°$; distance = 1 m.

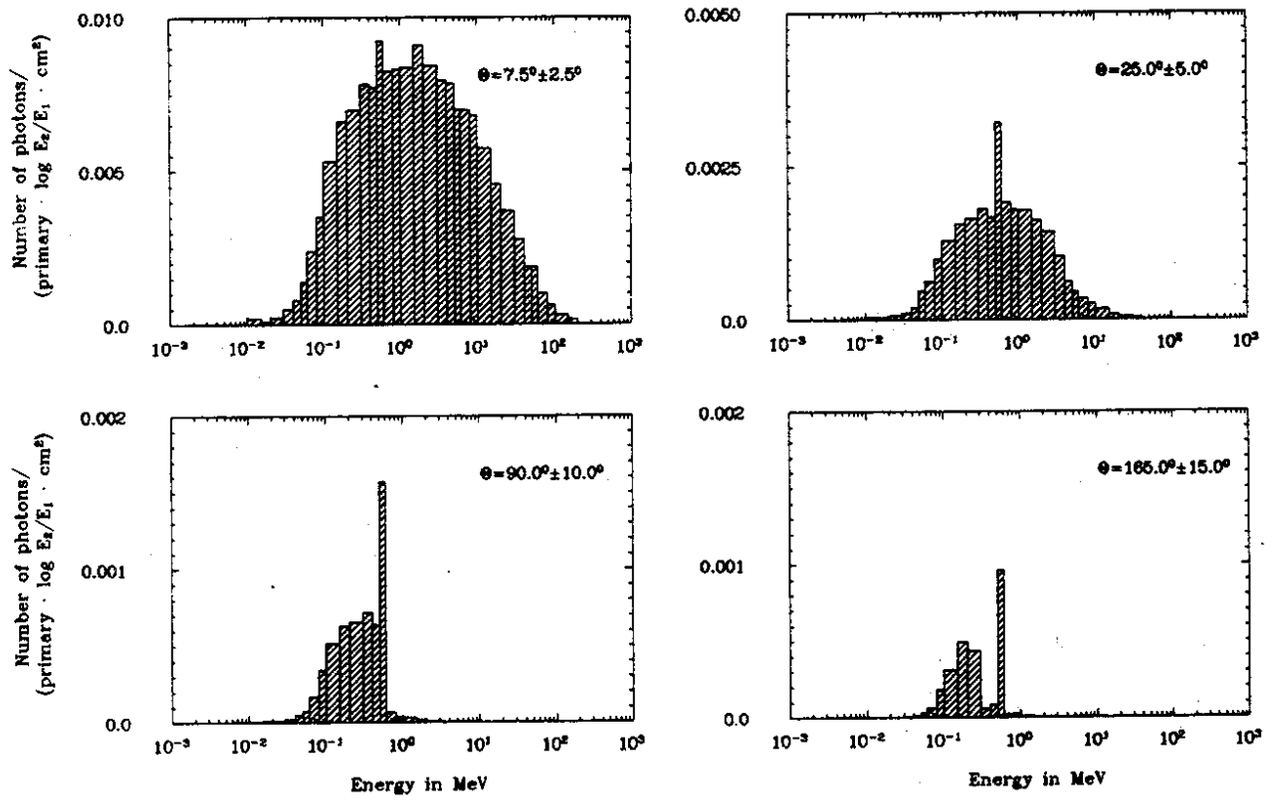

Figure 3: Spectra of secondary photons; primary energy = 5 GeV; iron target: d = 0.2 cm; $\varphi = -2°$; distance = 1 m.

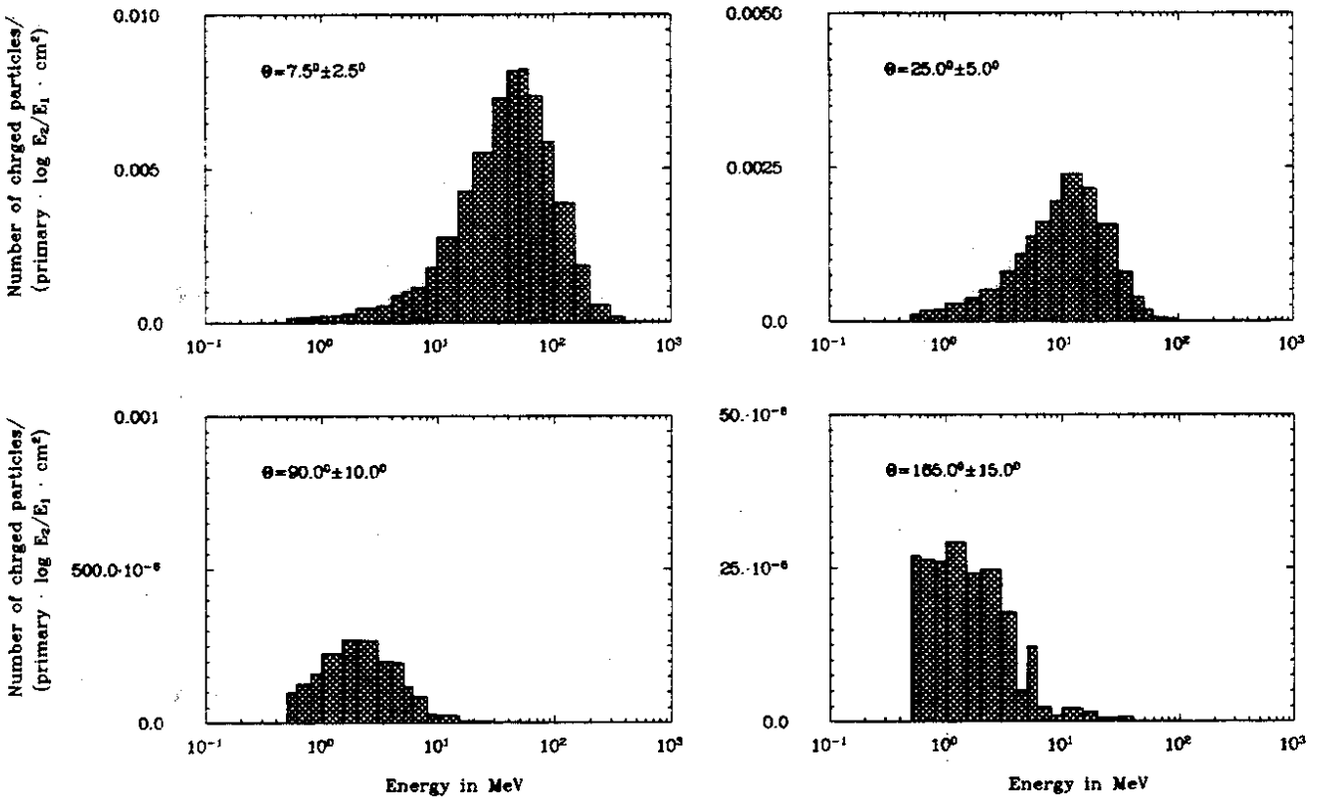

Figure 4: Spectra of secondary charged particles (electrons and positrons); primary energy = 5 GeV; iron target: d = 0.2 cm; $\varphi = -2°$; distance = 1 m.

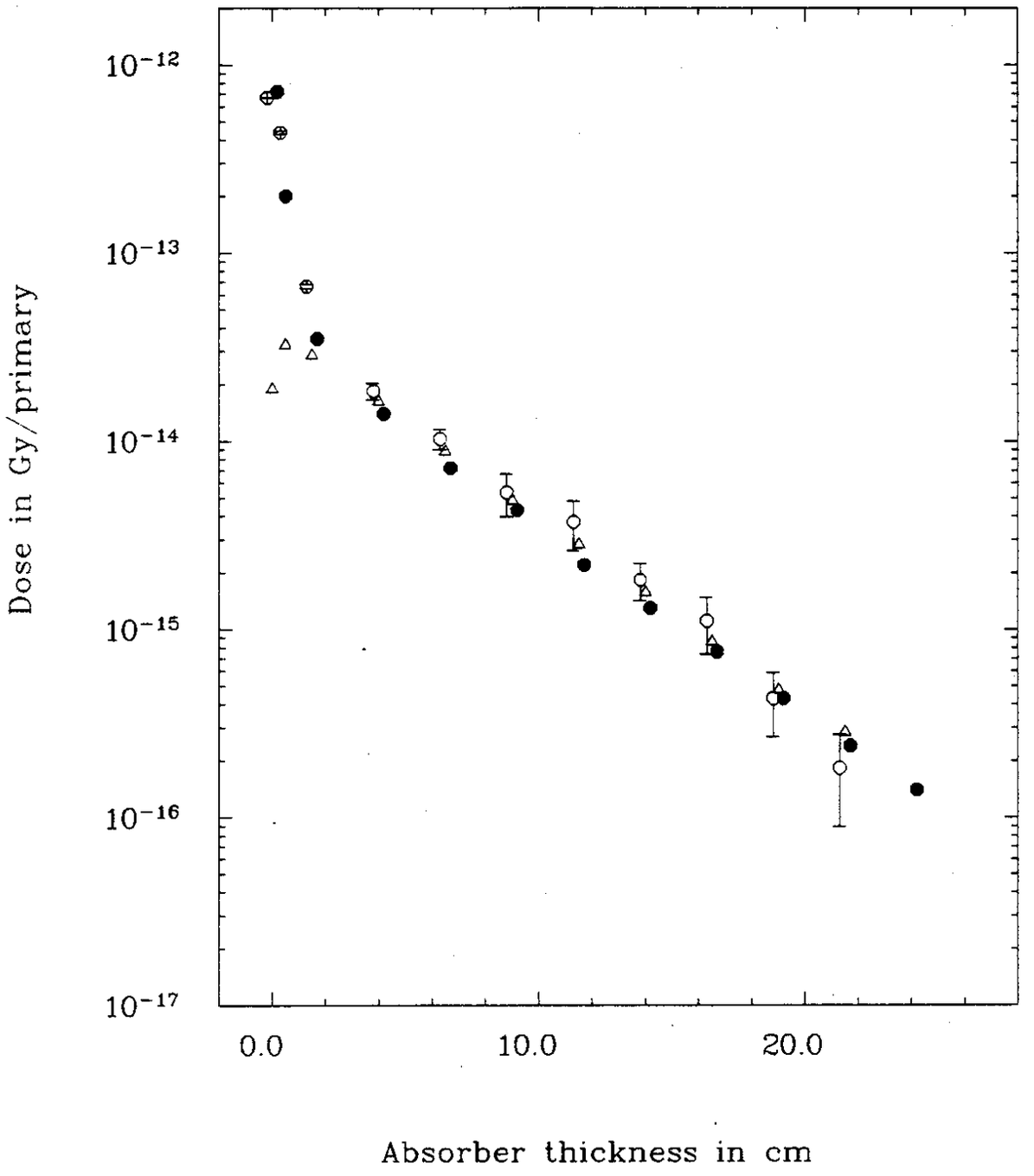

Figure 5: Absorption of stray radiation in iron; primary energy = 5 GeV; iron target: d = 0.2 cm; $\varphi = -2°$; observation: $\theta = 30°$; distance = 1 m; open circles: calculated doses; open triangles: calculated kerma; full circles: measured dose in Reference 1.

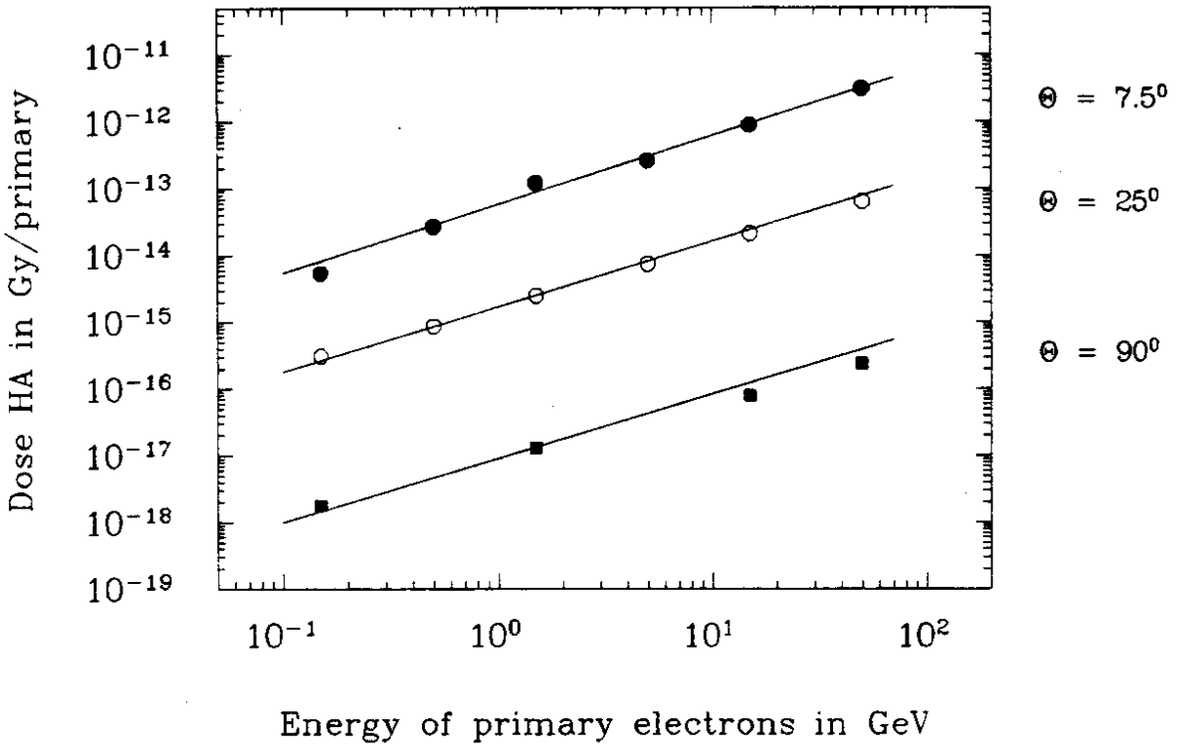

Figure 6: Dependence of source term H_A on primary energy; iron target: d = 0.2 cm; $\varphi = -0.5°$; distance = 1 m.

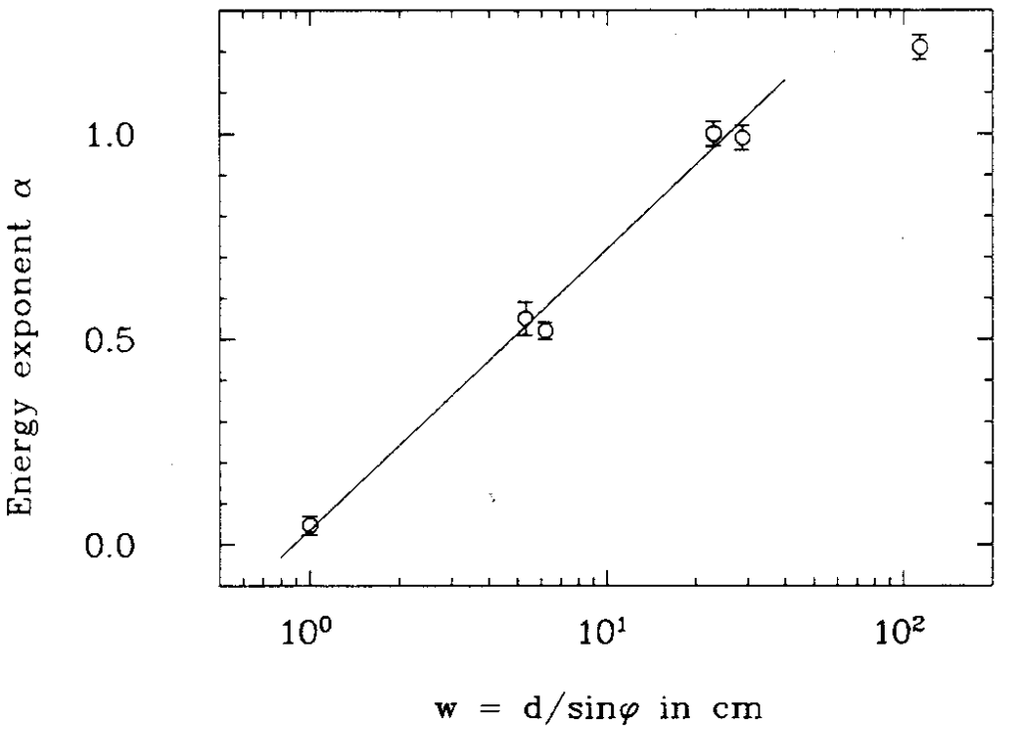

Figure 7: Dependence of the energy exponent α on the thickness w for iron targets.

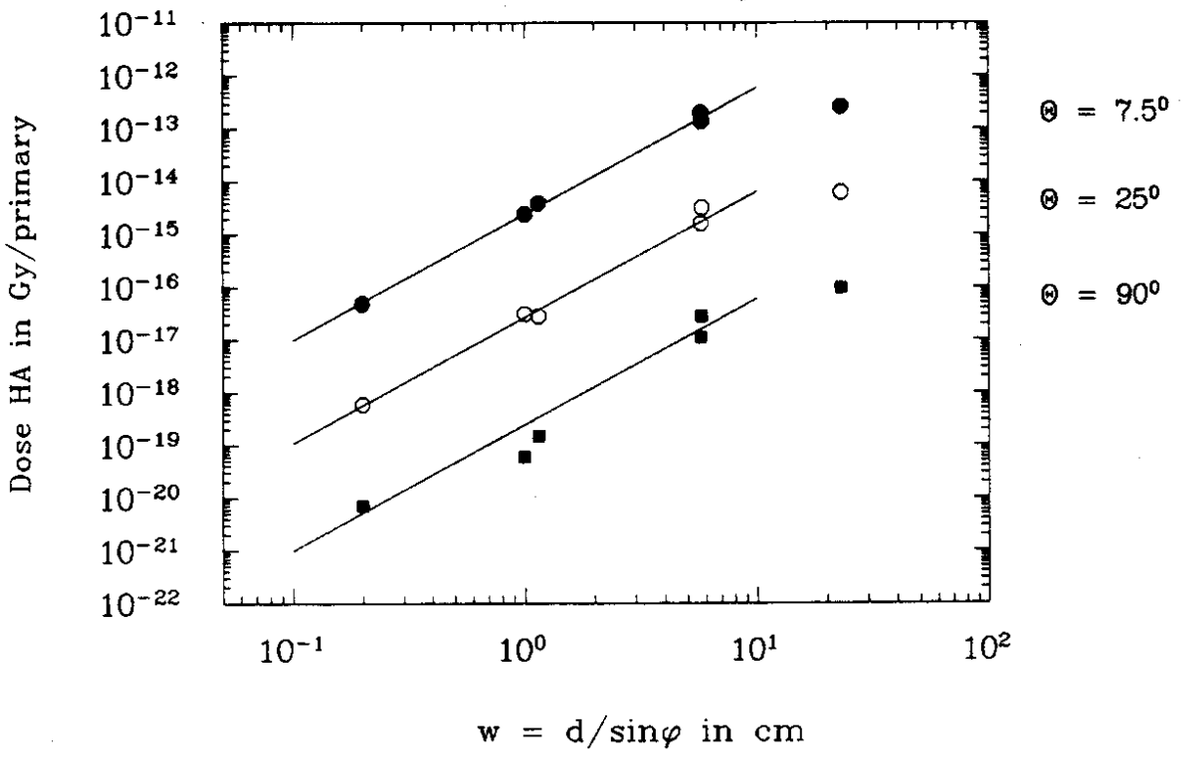

Figure 8: Dependence of source term H_A on the target configuration; primary energy = 5 GeV; iron target; distance = 1 m.

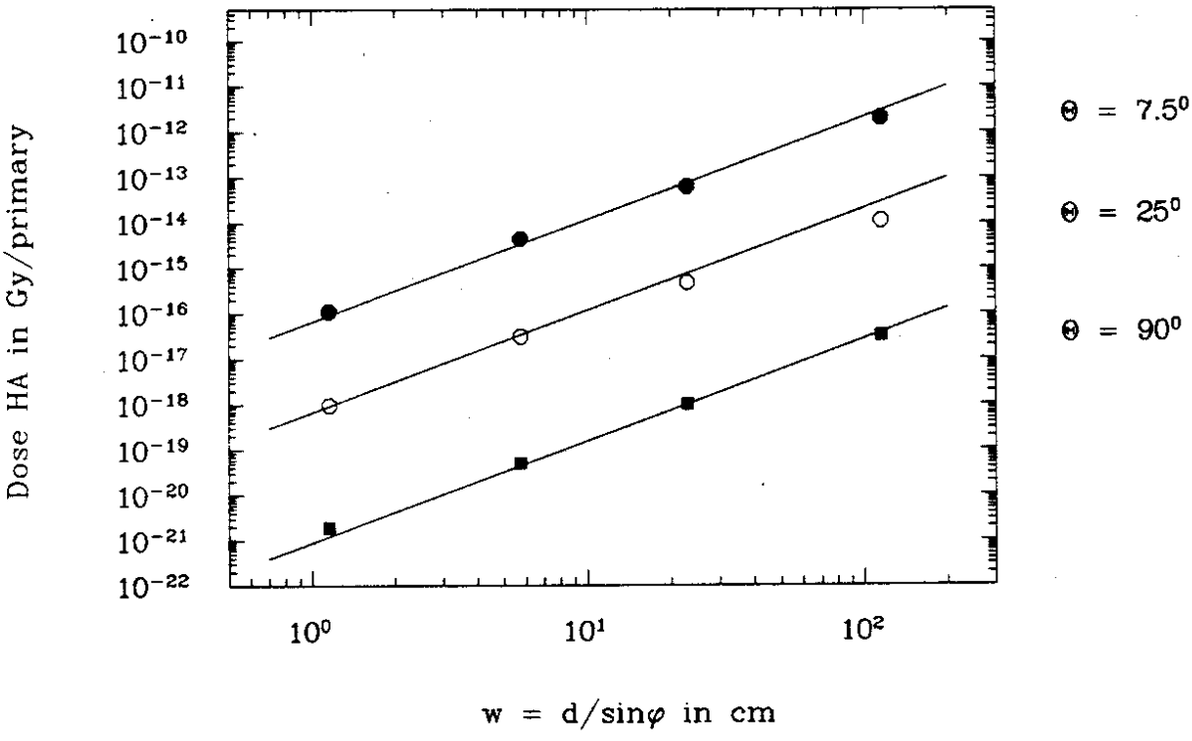

Figure 9: Dependence of source term H_A on the target configuration; primary energy = 5 GeV; aluminium target; distance = 1 m.